ICEMG 2023-XXXXX

Design of Dual-Rotor Dual-Stator Axial-Field Flux-Switching PM Motor with Low-Cogging Torque and Low-Torque Ripple

Fariba Farrokh[1], **Hossein Torkaman** [2], **Aboldazl Vahedi**[3], **Mahdi Banejad**[1]

[1] Faculty of Electrical Engineering, Shahrood University of Technology, Shahrood, Iran.
[2] Faculty of Electrical Engineering, Shahid Beheshti University, Tehran, Iran.
[3] Department of Electrical Engineering of Iran University of Science & Technology, Tehran, Iran.

Abstract
In this paper, the dual-rotor dual-stator axial field flux-switching PM (DR-DS-AFFSPM) topology is presented, designed, and analyzed to improve the cogging torque and torque ripple. The 12-pole dual-stator has been located on both sides of the 10-pole internal dual-rotor and phase-group concentrated-coil windings for the aim of increasing fault-tolerant capabilities. The 3D finite element method (3D-FEM) analysis is utilized for determining the main characteristics, such as the magnetic field distribution, the flux-linkage, back electromagnetic force, the cogging torque, the output torque, the torque ripple, and the losses in the internal dual-rotor DS-AFFSPM motor. A comparative analysis in the same condition is thoroughly made of the designed topology and related topology in literature, in order to determine the most effective structure such as traction applications based on torque density, torque ripple, cogging torque, and efficiency. The results show that, the low-cogging torque, low-torque ripple, high-torque density, and high-efficiency, of the internal dual-rotor DS-AFFSPM topology is a suitable candidate for traction applications.

Keywords: dual-stator axial field flux-switching machine, high-torque density, low-torque ripple, low-cogging torque, traction applications.

I. Introduction

The field flux-switching PM (FFSPM) machine is a type of brushless machine with bipolar stator flux, and all active sources, including concentric coil windings and PMs, are located in the stator and has a rotor similar to the rotor of the reluctance switch machine. The phase-group concentrated-coil windings is improved fault-tolerant capabilities [1].

The axial FFSPM motors have an advantage with the high-torque density as compared to the radial flux switching motors [2]. Recently, electrical propulsion systems demand high-torque density, high-efficiency, low-cogging torque, low-torque ripple, and fault-tolerant capabilities for traction applications. Therefore, AFFSPM motors are useful for traction applications when dealing with requirements [3-5].

A topology is suggested in [6], in which the 12/10 an external dual-rotor DS-AFFSPM machine; the chamfer of the stator slot and rotor pole width can result in the back-EMF waveform is improved and the cogging torque is reduced. A 12/13 external dual-rotor DS-AFFSPM that has a lower cogging torque and higher torque density is then proposed; the back-EMF waveform and cogging torque about the rotor offset angle β (elec.) make for better performance [7]. As well as, a structure of external dual-rotor DS-AFFSPM, and using an arc-shaped magnet decreases the cogging torque and the rated torque by regarding 61.8% and 6.22%, respectively [8].

A topology is proposed in [9], 6/4 an inner dual-rotor DS-AFFSPM machine, which has a torque density with the main idea of maintaining a phase shift of $\pm \pi$ electric radians between stators. A recent study [10] shows that a 12/10 external dual-rotor DS-AFFSPM motor for electric vehicle applications is then proposed. The rotor pole skewing is reduced the torque ripple and the amplitude of the back-EMF but it increases the cogging torque by 5.83%.

Despite the higher torque density, AFFSPM machines defect due to their configurations such as higher cogging torque. Methods such as slots/poles skewing, chamfer in the stator slot, and magnet segmentation are effective for improving the cogging torque in AFFSPM machines, but the torque density and back-EMF value be reduced [11-14]. More research has been done on the AFFSPM machines, which suffer from torque ripple. Methods such as tooth and PM skewing, rotor pole skewing, and various rotor shapes will are reduced the torque ripple [15].

According to the operating principles of the AFFSPM, an internal dual-rotor three-phase dual-stator AFFSPM has been designed. In which the phase-group concentrated-coil windings and skewing of the two rotor poles are used. The main characteristics, such as the magnetic field distribution, the flux-linkage, back electromagnetic force, the cogging torque, the output torque, the torque ripple, and the losses in the designed motor are predicted by the 3D-FEM. Finally, the internal dual-rotor DS-AFFSPM motor is compared with the external dual-rotor DS-AFFSPM motor. The check of motor performance is based on the same outer and inner diameters stator, length, and slots/rotor poles, in addition to the same rankings such as power and rated speed.

II. The Structure and Operation Principle

A. The presented Structure

Fig.1 shows the 3D exploded model, and it is the configuration of the internal dual-rotor DS-AFFSPM motor. Dual-stator with a U-shaped iron core and one-direction PM magnetization are positioned across from one another. The rotor yoke prevents the PM flux from

going to the second stator after it goes into the rotor in each stator.

B. The Operation Principle

A 2D model is presented in Fig. 2 to demonstrate the operational principles of the internal dual-rotor DS-AFFSPM structure. In (a), the PM flux connected to winding A1, leaving the rotor pole, is received by the stator teeth. Position 1 is the negative maximum mode. When the rotor rotates from position 1 to position 2. The PM flux is linked in coil A1 (b), out of the stator tooth and into the rotor pole. Position 2 is the positive maximum mode. When the rotor teeth meet the PM or slot of the stator, the position is zero modes. Therefore, a periodic EMF is induced and a bipolar flux-linkage is produced in windings with sinusoidal versus rotor positions.

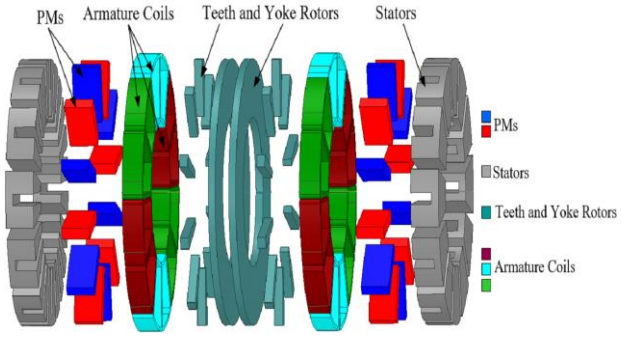

Figure 1. The 3D exploded view of internal dual-rotor DS-AFFSPM motor

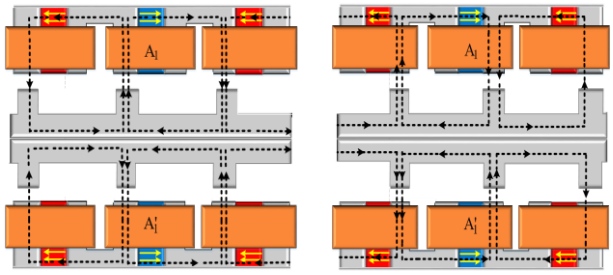

(a) Position 1 (b) Position 2

Figure 2. Two specific Operation principle in internal DR-DS-AFFSPM machines

In the after section, concerning the design equations, the dimensions of the internal dual-rotor DS-AFFSPM topology is obtained.

III. Design of DR-DS-AFFSPM Motor

A. Design Process

The output power equation of the DR-DS-AFFSPM motor, according to the reference [6], is defined as:

$$P_{out} = mE_m I_m \eta \tag{1}$$

$$P_{out} = \frac{\pi^3\sqrt{2}}{240}\frac{P_r}{P_s} K_l K_g \lambda\left(1-\lambda^2\right) A_s B_{g\max} \beta_i D_{so}^3 \eta \tag{2}$$

where m is the phase number and η is the efficiency. P_s is the stator tooth number and P_r is the rotor pole number. K_l is a leakage flux factor and K_g is the factor of the air-gap flux density distribution. λ is the ratio of the inner and outer diameters. As is the maximum current density and B_{gmax} is the peak value of the air-gap flux density. β_i is the area ratio of the stator tooth and stator tooth-slot unit. D_{so}, D_{si} are the stator outer and inner diameters, and nr is the speed of the rotor.

The output torque is expressed as:

$$T_{out} = \frac{\pi^2\sqrt{2}}{8}\frac{P_r}{P_s} K_l K_g \lambda\left(1-\lambda^2\right) A_s B_{g\max} \beta_i D_{so}^3 \eta \tag{3}$$

Infer (2), the stator outer diameter can be expressed as:

$$D_{so} = \sqrt[3]{\frac{240 P_{out} P_s}{\sqrt{2}\pi^3 P_r K_l K_g \lambda\left(1-\lambda^2\right) A_s B_{g\max} \beta_i n_r \eta}} \tag{4}$$

According to the machine design equations, motor parameters are achieved and are listed in Table 1.

Table 1. Design parameters of the internal DR-DS-AFFSPM motor

Number	Parameter	Symbol	Value
1	Slots / rotor poles	P_s/P_r	12/10
2	Rated speed (rpm)	n_r	1500
3	No. of Phases	m	3
4	Nominal power (W)	P	600
5	Current density(A/mm^2)	J	8

IV. FEM Analysis, Results, and Discussion

A. The Check of the Open-Circuit Magnetic Field Distribution

This section assesses the electromagnetic characteristics of the designed DR-DS-AFFSPM motor. Figure 3. illustrates the magnetic flux for different positions. In the poistion1, position 2, and position 3 modes, respectively, figures a, b, and c show flux-linkage. The presented model has maximum flux density of 1.8 T in position 1 and position 2, while it has a flux density of 0.6 T when there is position 3, and when the rotor teeth meet PMs.

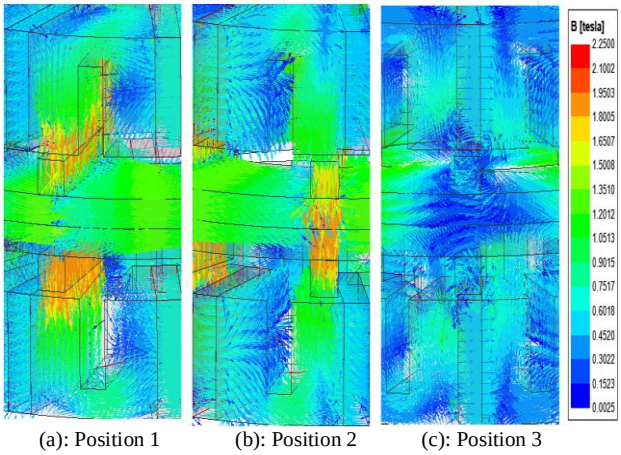

(a): Position 1 (b): Position 2 (c): Position 3

Figure 3. The 3D open-circuit magnetic flux vector of internal DR-DS-AFFSPM motor

B. Analysis of the Flux-Linkage and Induced Voltage Characteristics

When a sinusoidal current is followed in the windings, and according to how the back-EMF voltage is formed in figure 4, electromagnetic torque is produced. The three-phase open-circuit flux-linkage of the internal DR-DS-AFFSPM motor is shown in Figure 5. the maximum flux-linkage amplitude is 0.033 Wb. Figure 6. demonstrations the three-phase back-EMF sinusoidally for the rated speed (@1500 rpm) of the DR-DS-AFFSPM motor in accordance with figure 5. The motor has back-EMF amplitude of 52.09 V.

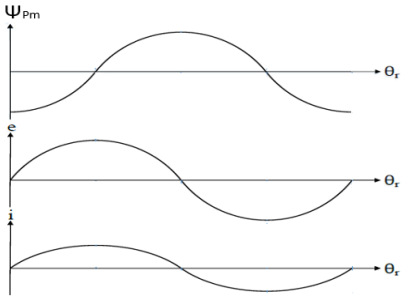

Figure 4. Operational principles of DR-DS-AFFSPM motor

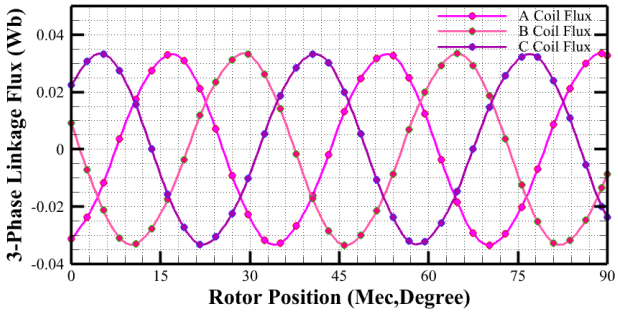

Figure 5. The flux-linkage in the three-phase of the internal DR-DS-AFFSPM motor

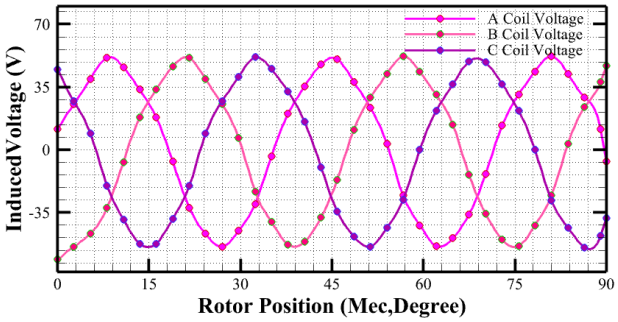

Figure 6. The back-EMF in the three-phase of the internal DR-DS-AFFSPM motor

C. The Cogging Torque and Out-Torque Analysis

Cogging torque is obtained from the energy stored in the magnetic field relative to the change in the angular position of the rotor when the current in the coils is zero.

$$T(\theta) = -\frac{\partial W(\theta)}{\partial \theta} \tag{5}$$

$$T(\theta) = -\frac{\partial}{\partial \theta}\left\{\frac{1}{4\mu_0}\left(D_{so}^2 - D_{si}^2\right)\int_0^{L_a}\int_0^{2\pi} G^2(z,\theta)B^2(\alpha,\theta)d\alpha dz\right\} \tag{6}$$

where μ_0, L_a, and α are the air permeability, length of stator, and the relative angular position between the stator and the rotor, respectively. In addition, $G(z, \theta)$ and $B(\alpha, \theta)$ are the directivity function of the air gap and the check function of the air gap flux, respectively. Therefore, it is possible to reduce the cogging torque by increasing the number of cogging torque vibrations in an electrical cycle or by optimizing parameters such as $G(z, \theta)$ and $B(\alpha, \theta)$. Since the PM is embedded in the stator of the motor, it is not easy to change the structure of the inner diameter of the stator near the air gap, and the flux density function of the air gap $B(\alpha, \theta)$ cannot be changed. Therefore, the reduction of cogging torque can be achieved by changing the air gap guidance function $G(z, \theta)$.

In PM motors, pole or slot skewing has been used to reduce the cogging torque of the motor and the effect of cogging torque weakening has been revealed. Since the rotor of the FSPM motor is salient, the skewing of the rotor is much easier than that of the conventional PM motor. The skewing of the rotor pole is equivalent to changing the variables of the $G(z, \theta)$ function in equation (5) in order to reduce the cogging torque. It is equivalent to increasing the length of the air gap of the motor and increasing the reluctance in the magnetic circuit, which causes a decrease in the amplitude of the back-EMF.

Figure. 7(a) and 7(b) demonstrate the rotor configuration of the presented model 1 and the model 2 with rotor pole skewing 0 dge and -1 dge, respectively. However, the skewing of the rotor pole reduces the overlap between the rotor poles and the stator teeth.

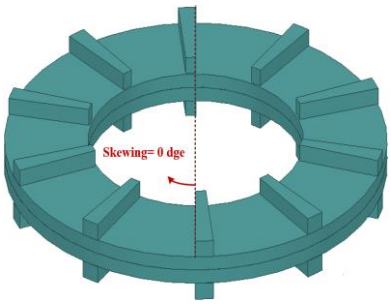

(a): Model 1: Rotor pole skewing= 0 dge

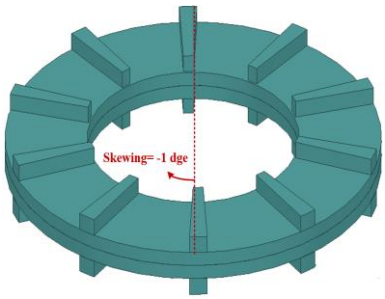

(b): Model 2: Rotor pole skewing= -1 dge

Figure 7. The Rotor pole of the internal DR-DS-AFFSPM motors

Figure 8. shows the cogging torque of the internal DR-DS-AFFSPM motor. In presented model 2 is the skew of the rotor pole of -1dge compared to the model 1. The model 1 and model 2 have cogging torques of 2.24, and

2.02 Nm, respectively. Figure 7 shows the internal DR-DS-AFFSPM models' output torque at 8 A/mm^2 and 1500 rpm. The model 2 increased by 7.75 percent to 5 Nm, compared to the model 1 to 4.64 Nm.

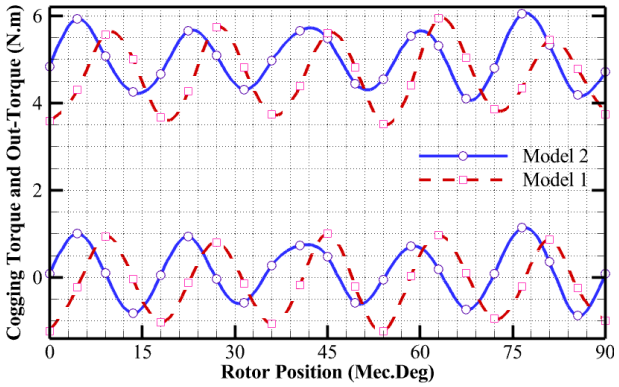

Figure 8. The cogging torque and out-torque of the internal DR-DS-AFFSPM motor

D. The Torque Ripple Analysis

Equation (7) expresses the output torque ripple:

$$\%TR = \frac{T_{\max} - T_{\min}}{T_{avg}} \times 100\% \quad (7)$$

where T_{max}, T_{min}, and T_{avg} are the maximum, minimum, and average torque, respectively. The model 1 has higher torque ripple at 52.15%, followed by the model 2 at 38.8%, down 25.6%.

V. The Comparative Study

A comparison of the presented models' operational characteristics with some machines such as two models of external dual-rotor DS-AFFSPM motor [10] as illustrated in Figure 8. Table 2 contains a list of these topologies. The two models under comparison and the models suggested in [10] share characteristics like the geometric shape, and the size of the stator slot are the same in the four models. Their only difference is how to put the dual-stator and the dual-rotor together.

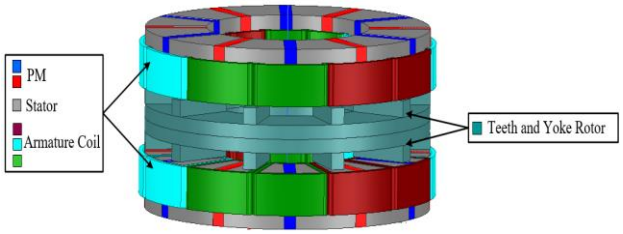

(a): Internal DR-DS-AFFSPM Model

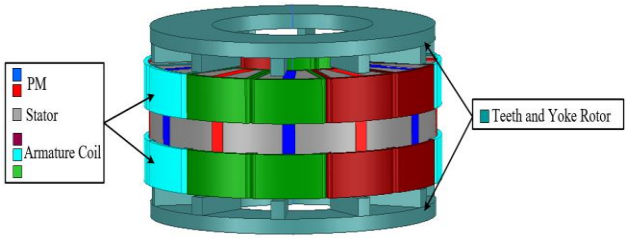

(b): External DR-DS-AFFSPM Model [10]

Figure 9. The models of the DR-DS-AFFSPM motors listed in the operational comparison

The amplitude of the back-EMF of the presented model 2 and model 2 [10] at 50.27 V, down 3.5%, and 47.2 V, down 6.05%, respectively. Because of its increasing length of the air gap with rotor pole skewing.

In comparison to [10] model 1 and 2, the presented model 2 has, respectively, 18.81%, and 25.74% lowest cogging torque. In comparison to the presented model 2, the cogging torques of the presented model 1 decreased by 9.82%. In comparison to the presented model 1, the average output torque of the presented model 2 increased by 7.75%. The presented model 2's minimum torque ripple in the three models is 38.8%.

The presented model 2 has the same power of 0.785 KW and out-torque of 5 Nm; when compared to [10] model. Although it has the lowest cogging and ripple torque than the [10] models, the efficiency of the in [10] model 2 is lower by 0.06%. The presented model 1 has higher losses at 71.61 W, followed by the presented model 2 at 70.08 W, down 2.13%. Meanwhile, [10] model 1 and model 2 have lowest losses at 70.05 W and 69.4 W, respectively.

Table 2. Performance comparison of the DR-DS-AFFSPM topologies with other topologies

Number	Parameter	Model 1	Model 2	Model 1[10]	Model 2 [10]
1	Slots/rotor poles	12/10			
2	Current density (A/mm^2)	8			
3	Rated speed (rpm)	1500			
4	Back-EMF (V)	52.09	50.27	50.24	47.12
5	Cogging torque (Nm)	2.24	2.02	2.4	2.54
6	Torque (Nm)	4.64	5		
7	Torque density (Nm/L)	4.33	4.67		
8	Power (KW)	0.72	0.78		
9	Torque ripple (%)	52.18	38.8	58.91	48.89
10	Total losses (W)	71.61	70.08	70.05	69.4
11	Efficiency (%)	90.95	91.8	91.76	91.86

VI. Conclusion

This paper has presented, fault-tolerant internal DR-DS-AFFSPM in which the phase-group concentrated coil windings and rotor pole skewing are utilized. The internal DR-DS-AFFSPM topology is compared for traction applications to improve the torque density and torque ripple. The findings show that, in comparison to the model presented internal dual-rotor DS-AFFSPM has both the lowest cogging torque and less ripple torque because of the two attached rotor yokes. However, the external dual-rotor DS-AFFSPM [10]

model has two separated rotor yokes, which have both the bigger cogging torque and higher ripple torque than the model presented. The presented model 2 has a high-torque density of 4.67 Nm/L, which is an increase of 1.26% in comparison to the presented model 1. Due to its lowest cogging torque, lowest torque ripple, and high efficiency, the presented internal dual-rotor DS-AFFSPM motor is a suitable candidate for traction applications among the three models because it has higher torque density.

Nomenclatures

P_s The stator tooth number
P_r The rotor pole number
η The efficiency
A_s The electrical load
D_{so} The stator outer diameter
D_{si} The stator inner diameter
L_a The length of stator
K_l The leakage flux factor
K_g The factor of air-gap flux density distribution
β_i The area ratio of stator tooth and stator tooth-slot unit
λ The ratio of the inner diameter and the outer diameter of the stator

Greek symbols

μ_0 Air permeability

References

[1] X. Xue, W. Zhao, J. Zhu, G. Liu, X. Zhu and M. Cheng, "Design of Five-Phase Modular Flux-Switching Permanent-Magnet Machines for High Reliability Applications," in IEEE Transactions on Magnetics, vol. 49, no. 7, pp. 3941-3944, July (2013)

[2] X. Zhang, W. Zhang, X. Liang and P. Lu, "Performance analysis and comparison for two topologies of flux-switching permanent magnet machine," in CES Transactions on Electrical Machines and Systems, vol. 4, no. 3, pp. 190-197, Sept. (2020)

[3] L. Xu, X. Zhu, W. Fan, C. Zhang, L. Zhang and L. Quan, "Comparative Analysis and Design of Partitioned Stator Hybrid Excitation Axial Flux Switching PM Motors for In-Wheel Traction Applications," IEEE Transactions on Energy Conversion, vol. 37, no. 2, pp. 1416-1427, (2022)

[4] J. Si, T. Zhang, R. Nie, C. Gan and Y. Hu, "Comparative Study of Dual-Rotor Slot less Axial-Flux Permanent Magnet Machines With Equidirectional Toroidal and Conventional Concentrated Windings," in IEEE Transactions on Industrial Electronics, vol. 70, no. 2, pp. 1216-1228, Feb. (2023)

[5] H. Torkaman, A. Ghaheri and A. Keyhani, "Design of Rotor Excited Axial Flux-Switching Permanent Magnet Machine," in IEEE Transactions on Energy Conversion, vol. 33, no. 3, pp. 1175-1183 (2018)

[6] L. Hao, M. Lin, W. Li, H. Luo, X. Fu, and P. Jin, "Novel dual-rotor axial field flux-switching permanent magnet machine," IEEE Transactions on Magnetics, vol. 48, no. 11, pp. 4232–4235 (2012)

[7] W. Zhao, T. A. Lipo, and B. I Kwon, "A novel dual-rotor, axial field, fault-tolerant flux-switching permanent magnet machine with high-torque performance," IEEE Transactions on Magnetics, vol. 51, no.11, pp. 3–6 (2015)

[8] M. Aakif Baig, J. Ikram, A. Iftikhar, S. S. H. Bukhari, N. Khan and J. -S. Ro, "Minimization of Cogging Torque in Axial Field Flux Switching Machine Using Arc Shaped Triangular Magnets," IEEE Access, vol. 8, pp. 227193-227201 (2020)

[9] J. H. Kim, Y. Li and B. Sarlioglu, "Novel Six-Slot Four-Pole Axial Flux-Switching Permanent Magnet Machine for Electric Vehicle," IEEE Transactions on Transportation Electrification, vol. 3, no. 1, pp. 108-117 (2017)

[10] F. Farrokh, A. Vahedi, H. Torkaman, and M. Banejad, "Design of Axial Field Flux Switching Motor with Improved Torque Ripple for Electric Vehicle Applications", The 9th Iranian Conference on Renewable Energy & Distributed Generation, Mashhad, https://civilica.com/doc/1465037 (2022)

[11] D. Xu, X. Jiang, Y. Tu, N. Li, and Q. Li, "Investigation of cogging torque reduction for a 6/10 hybrid axial field flux-switching permanent magnet machine by harmonic field current injection," IET Electric. Power Application., vol. 14, no. 12, pp. 2499–2506 (2020)

[12] Z. Xing, X. Wang, and W. Zhao, "Cogging torque reduction based on segmented skewing magnetic poles with different combinations of pole-arc coefficients in surface-mounted permanent magnet synchronous motors," IET Electric. Power Application, no. July 2020, pp. 200–213 (2021)

[13] Z. Xing, X. Wang, and W. Zhao, "Cogging torque reduction based on segmented skewing magnetic poles with different combinations of pole-arc coefficients in surface-mounted permanent magnet synchronous motors," IET Electric. Power Application, no. July 2020, pp. 200–213 (2021)

[14] T. Jahns, "Getting Rare-Earth Magnets Out of EV Traction Machines: A review of the many approaches being pursued to minimize or eliminate rare-earth magnets from future EV drivetrains," IEEE Electrification Magazine, vol. 5, no. 1, pp. 6-18 (2017)

[15] H. Jang, H. Kim, H. C. Liu, H. J. Lee, and J. Lee, "Investigation on the torque ripple reduction method of a hybrid electric vehicle motor," Energies, vol. 14, no. 5, (2021)